nature physics

Article

https://doi.org/10.1038/s41567-025-02835-7

Topological dynamics of rapid non-planar gaits in slithering snakes

Received: 15 September 2020

Accepted: 19 February 2025

Published online: 10 April 2025

Check for updates

N. Charles[1,7], R. Chelakkot[2,7], M. Gazzola[3], B. Young[4] & L. Mahadevan[5,6]

Snakes exhibit a wide variety of gaits, including gliding in air and sidewinding on land, which is particularly notable for its out-of-plane motion. Here we report the observation of another non-planar gait used as an escape strategy from threatening situations by juvenile anacondas (*Eunectes notaeus*), which we refer to as the S-start due to its shape. In this transient mode of locomotion, the snake writhes and bends out of the plane while rolling forward about its midsection without slippage. To quantify our observations, we develop a model for an active non-planar filament that interacts anisotropically with a frictional substrate. We demonstrate that locomotion is due to a propagating localized pulse of a topological quantity—the link density. A two-dimensional phase space characterized by scaled body weight and muscular torque shows that relatively light juveniles are capable of S-starts, whereas heavy adults are not, consistent with our experiments. We also show that a periodic sequence of S-starts naturally leads to a sidewinding gait.

Snakes exhibit a wide variety of gaits, of which the most commonly described ones classically are rectilinear motion[1,2], periodic undulation[1,3–9] and sidewinding[1,10–12] on land. However, there has been increasing recognition that this classification is incomplete[13], and needs to be broadened to include more complex gaits that arise in different environments, and include modes of arboreal climbing[14], gliding in air[15] and traversing uneven terrain[16,17]. Furthermore, there is a recognition that snakes use a range of transient modes such as concertina locomotion[1,18] and various striking and escape lunges[19–21], depending on the species, physical environment and behaviour, going well beyond the simple steady states that are often easier to study. Complementing these experimental approaches have been attempts to describe steady-state gaits theoretically[6–9] as they are easier to model and allow one to ask questions about optimality and locomotor efficiency[22], with relevance for robotics.

Here we describe and quantify a transient non-planar mode observed in newborn and juvenile yellow anacondas (*Eunectes notaeus*) that gives the snake a large forward velocity, often used defensively to escape a threatening situation; this is particularly noteworthy, since adult anacondas are known to be very slow moving. We dub this mode the S-start since the snake forms an S shape, analogous to a transient manoeuvre commonly seen in juvenile fish, the C-start[23,24]. To execute the S-start, the snake forms an S shape consisting of three roughly co-linear segments connected by two tightly curved regions (Fig. 1a). Motion begins when the two curved segments are lifted off the ground. Simultaneously, the outer, parallel straight segments move along the ground even as the middle straight segment remains stationary. This causes the curved segments to travel along the snake (Supplementary Video 1). Thus, the snake effectively moves by propagating a spatially localized region that is bent and twisted out of the plane. The forward propulsion of the snake arises when this non-planar region moves through the snake even as most of its body is in contact with the surface and does not slip at all. This leads to the snake moving forward without sliding on the surface, similar to how a wrinkle in a rug can be moved

[1]School of Engineering and Applied Sciences, Harvard University, Cambridge, MA, USA. [2]Department of Physics, Indian Institute of Technology Bombay, Mumbai, India. [3]Department of Mechanical Science and Engineering, National Center for Supercomputing Applications, Carl R. Woese Institute for Genomic Biology, University of Illinois at Urbana-Champaign, Urbana, IL, USA. [4]Department of Anatomy, A.T. Still University of Health Sciences, Kirksville College of Osteopathic Medicine, Kirksville, MO, USA. [5]School of Engineering and Applied Sciences, Cambridge, USA. [6]Departments of Physics and of Organismic and Evolutionary Biology, Harvard University, Cambridge, MA, USA. [7]These authors contributed equally: N. Charles, R. Chelakkot.
e-mail: lmahadev@g.harvard.edu

https://doi.org/10.1038/s41567-025-02835-7

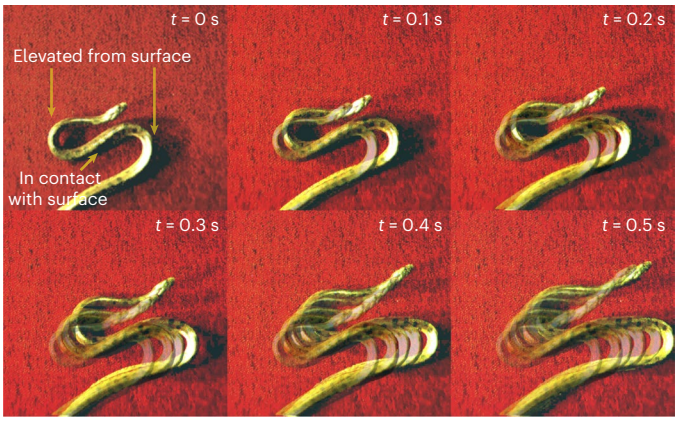

Fig. 1 | S-start of juvenile anaconda (*E. notaeus*) on a red synthetic turf. The starting point of locomotion is an S shape including three co-linear regions, connected by two curved regions that are elevated from the contact surface (as observable from the shadow cast on the substrate) as the middle, straight segment pushes down against the surface. Series of overlaid time-lapse images separated by 0.1 s show the S-start—the snake moves rightwards as a localized pulse of non-planar bends propagates through the snake (Supplementary Video 1).

by rolling through it[25]. As the snake propels itself forward, the S shape flows along its length, until one end comes off the ground, terminating this transient mode of motility (Fig. 1b–f). Globally, this leads to motion parallel to the direction of the snake's head and is reminiscent of sidewinding[1,12], and as we will see, forms the elemental building block from which many non-planar gaits including sidewinding may be constituted.

Lifting its body as it moves allows the snake to minimize frictional losses, but comes with a cost—the snake has to overcome gravity and move out of the plane to do so. We expect slender snakes or those with relatively stronger musculature to be able to achieve this, whereas thicker snakes or those with relatively less musculature/more bone are unable to do so[26]. For a snake of mass density ρ and diameter a, the maximum length ℓ that can be supported out of the plane is determined by a balance between the active torque that deforms the snake and the passive gravitational torque required to lift the snake by a height $h \approx a$. The enabling active muscular torque scales as $m \approx \Gamma a^2 h f(\phi)$, where Γ is the maximum muscular stress, $\phi \in [0,1]$ is the fraction of tissue that is muscle and $f(\phi)$ is a monotonic dimensionless function of ϕ, whereas the passive gravitational torque scales as $\sim \rho g a^2 \ell^2$ (where g is the acceleration due to gravity). Equating the two yields the scaling law $\ell \sim \sqrt{\Gamma a f(\phi)/(\rho g)}$. As the snake grows in girth, due to a concomitant increase in bone mass[27–29], its internal muscle fraction $f(\phi)$ decreases, so that the length it can support off the ground decreases, and the S-start becomes physically unattainable. Indeed, our study of locomotion in three newborn, five juvenile and two adult anacondas with a range of lengths and weights (Supplementary Section I) reveals that all the newborn and juvenile anacondas can move using the S-start, whereas none of the adult anacondas exhibit this type of locomotion.

To understand these observations quantitatively, we model the snake (Fig. 2a) as an active elastic filament interacting frictionally with a planar substrate[30]. The filament is assumed to have a circular cross-section of diameter a and length L with aspect ratio $L/a = 50$. The axis is parameterized by material coordinate s, and the shape of the snake at a particular time t can be characterized in terms of a local position vector $\mathbf{r}(s,t)$ and an associated material orthonormal coordinate system $\{\mathbf{d}_1(s,t), \mathbf{d}_2(s,t), \mathbf{d}_3(s,t)\}$. We assume that the filament has a passive bending rigidity B and twisting rigidity C, and we further neglect extensional and shear deformations of the filament—a reasonable assumption for long slender elastic objects; therefore, s becomes the arc length and $\mathbf{d}_3(s,t)$ is the tangent to the centerline of the snake. Since the filament is capable of exerting muscular couples along its body, we define an active torque vector $\mathbf{m} = \Sigma_{i=1}^{3} \mathbf{m}_i \mathbf{d}_i$ (Fig. 2a), associated with the two bending modes and one twisting mode of the filament at each cross-section. Then, the motion of the filament is determined via the balance of linear and angular momenta governed by the equations $\rho a^2 \partial \mathbf{v}(s,t)/\partial t = \partial \mathbf{f}(s,t)/\partial s + \mathbf{F}_e(s,t)$ and $\mathbf{I}\partial \boldsymbol{\omega}(s,t)/\partial t = \partial \mathbf{M}(s,t)/\partial s + \mathbf{d}_3 \times \mathbf{f}$. Here ρ is the density of the filament, $\mathbf{v} = \partial \mathbf{r}/\partial t$ is the local filament velocity, $\mathbf{f}$ is the vector of the force resultants at a cross-section, $\boldsymbol{\omega}$ is the local angular velocity of filament rotation, $\mathbf{I}$ is the moment of inertia of the cross-section (assumed to be circular), $\mathbf{M} = \mathbf{B}\mathbf{k}(s,t) + \mathbf{m}(s,t)$ is the sum of the passive elastic torques (associated with the vector of bending and twisting strains $\mathbf{k}(s,t)$ and the matrix of bending and twisting stiffnesses $\mathbf{B} = \mathrm{diag}(B, B, C)$), and the active muscular torques $\mathbf{m}(s,t)$. Here $\mathbf{F}_e$ is the external force on the filament associated with gravity and frictional interactions with the ground (Supplementary Section II). We assume that the filament interacts with the substrate frictionally, with a finite friction coefficient that is anisotropic. Assuming $\mu_f < \mu_b < \mu_s$ to be the coefficients of kinetic friction in the forward, backward and sideways directions, respectively, we choose $\mu_f{:}\mu_b{:}\mu_s = 1.1{:}1.4{:}2$, based on previous experimental data[7].

To complete the mathematical formulation of the problem, we need to specify some boundary conditions, which correspond to the ends of the snake being free of forces and moments. We also need to specify the active moment $\mathbf{m}(s,t)$, and note that S-start shows that the snake has two localized bends associated with the in-plane curvatures ($\mathbf{m}_2$) at locations I and III, and one localized bend associated with out-of-plane curvature at the contact zone in the central segment that is pressed downwards with an out-of-plane torque ($\mathbf{m}_1$) at location I (Fig. 2a). To model this arrangement of localized bending, we assume that the three active muscular torques are localized with a magnitude $m \approx \Gamma a^3 \mathrm{e}^{-(s-s_0-v_m t)^2/(2\sigma^2)}$, where Γ is the maximum magnitude of the muscular stress, s_0 is the initial location of the torque and σ is the axial scale over which the torque acts. We discretize the filament, and solve the associated discretized governing equations using the frictional contact model and numerical integration scheme given elsewhere[31].

In Fig. 2b, we show that these three localized torques move uniformly along the filament towards the tail with speed v_m relative to the body, causing a pulse-like travelling wave that propels the filament parallel to itself with speed $v_s = \mathbf{v}_{cm} \cdot \mathbf{x}_h$ ($\mathbf{x}_h$ is the unit vector associated with the direction of the head $s = 0$ and $\mathbf{v}_{cm}$ is the centre-of-mass velocity of the snake; Supplementary Video 2). Eventually, the active torques reach the tail and the whole filament straightens out. In Fig. 2c, we plot the local elevation of segments along the filament, showing that the travelling pulse corresponds to a small localized region of contact pushed down into the substrate as the curved regions are elevated above the surface. In Fig. 2d, we plot the local speed of the filament, $|\mathbf{v}|$, showing that the middle section at location III never slips relative to the surface, whereas the other regions move uniformly through this region.

The localized pulse that underlies the S-start has a topological interpretation that stems from recognizing that the non-planar shape and motion of a filament can be characterized in terms of the Călugăreanu–White–Fuller (CFW) theorem[32] relating the topological link (Lk) to the twist (Tw) and writhe (Wr) via the formula Lk = Tw + Wr for any closed filament. In this theorem, Lk quantifies the average number of oriented crossings of the edges of a ribbon[33], Wr is an integral measure of the out-of plane bending of a ribbon centerline[34] and Tw is the integrated rotation of an edge of the ribbon around the centerline (Supplementary Section IV). Here we apply these quantities to our open-ended active filament by treating the filament centerline $\mathbf{r}(s,t)$ and director vector $\mathbf{d}_1(s,t)$ as a mathematical ribbon (Supplementary Section IV). In Fig. 3a, we show the Wr of the snake body at a single moment during the simulated motion; light, muscular snakes show much more Wr than heavier, less muscular snakes. In Fig. 3b, we show that the scaled forward snake speed (averaged over a full motion cycle) is small for low values of Wr because of the effects of friction, as well as

https://doi.org/10.1038/s41567-025-02835-7

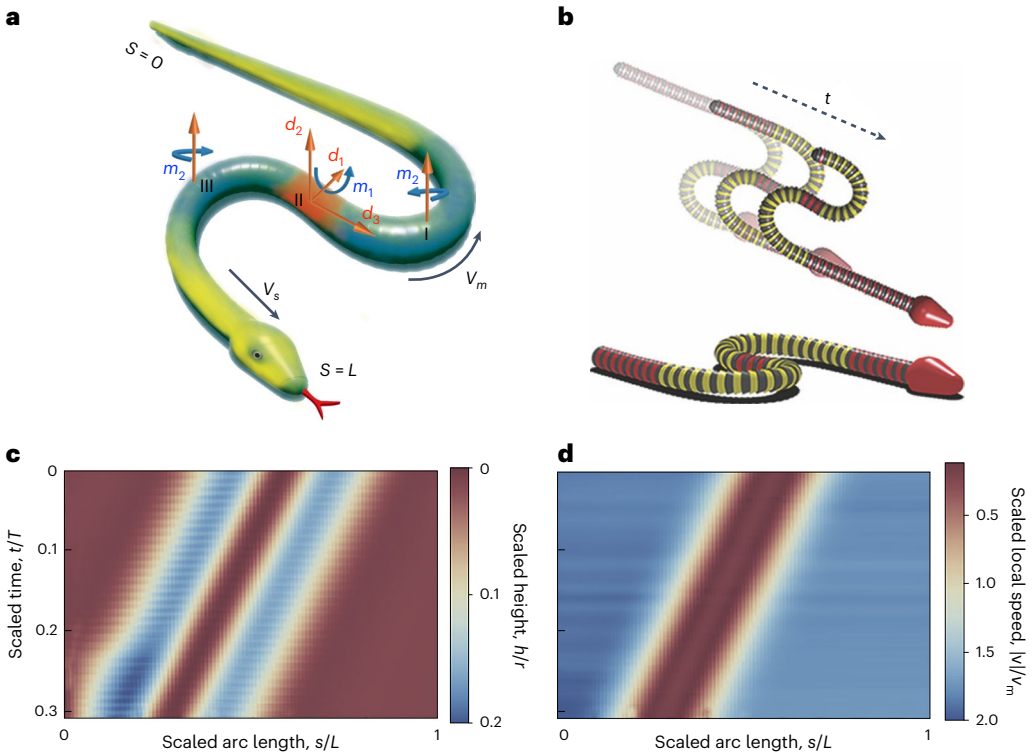

Fig. 2 | Biophysical model of the S-start. a, Schematic showing localized in-plane torques at locations I and II and a localized out-of-plane torque at III, which propagate from head to tail synchronously at speed v_m. The velocity of the snake's centre of mass v_s points parallel to the head direction. The orthonormal body-fixed material coordinate system is denoted by ($\mathbf{d}_1$, $\mathbf{d}_2$, $\mathbf{d}_3$), with respect to which ($\mathbf{m}_1$, $\mathbf{m}_2$, $\mathbf{m}_3$) indicates the localized muscle torques. **b**, Top: numerical simulations capture the dynamics of S-start (Supplementary Section II and Supplementary Video 2), showing how the snake moves towards the right by propagating in an S shape along itself with time t. Bottom: simulation snapshot shows the filament bending and writhing out of the plane. **c**, Kymograph (space–time plot) of the local vertical elevation (h/r), where r is the radius of the rod, as a function of scaled arc length (s/L), relative to the total length of the snake L, and scaled time (t/T), relative to a characteristic time $T = L/v_m$ shows that it is non-zero at two locations (I and III; blue) and vanishes elsewhere (brown), that is, the snake is stationary relative to the ground almost everywhere. **d**, Kymograph (space–time plot) of the local speed with respect to the substrate ($|\mathbf{v}|/v_m$), where v_m is the speed of the localized pulse. The speed is uniform almost everywhere and nearly zero in region II.

small for large values of Wr because the snake tends to flail and lift off from the ground. However, the speed is maximized for an intermediate value of Wr. In Fig. 3c, we plot the scaled snake forward speed v_s/v_m relative to the ratio of the body weight to muscular force, $\rho g L^2/\Gamma a$, by recombining the results of Fig. 3a,b. We see that the maximum forward speed is achieved for the weight and muscle that produce the optimal Wr in the snake body corresponding to a controlled three-dimensional snake body just short of inertial flailing.

To quantify the role of non-planar bending and writhing in the snake body during motion, we use local densities of Lk, Tw and Wr, denoted by λ, τ and ω, respectively, and defined by $\mathrm{Tw} = \int_0^L \tau(s)\mathrm{d}s$, $\lambda(s) = \mathrm{Lk}(\mathbf{r}([s, s+\delta]))/\delta$ and $\omega = \mathrm{Wr}(\mathbf{r}([s, s+\delta]))/\delta$, where $\mathbf{r}([s, s+\delta])$ denotes the section of the snake centerline for which the arc length coordinate lies in the range $[s, s+\delta]$, choosing $\delta = L/10$, determined empirically (Supplementary Section II and Supplementary Video 2). In the S-start, $\lambda(s,t) \neq 0$ in a small zone, and as the snake moves forward, $\lambda(s,t)$ translates along the body without changing its amplitude profile. By contrast, for friction-dominated locomotion, $\lambda_{\mathrm{friction}}(s,t) \neq 0$ and is small over most of the snake body, but during unstable flailing, $\lambda(s)$ shows no coherent pattern in space–time. Together, these observations show that a successful S-start has a simple topological interpretation: the snake must have a threshold, localized link current moving from its head to its tail.

To characterize the feasibility of the S-start in terms of the snake's morphology and musculature, we characterize a phase space in terms of ratio of the body weight to elastic forces, $\rho g a^2 L^3/B$, and the ratio of muscular forces to elastic forces, $\Gamma a^3 L/B$. In Fig. 3d, we see that in a relatively light snake that is overpowered, inertia dominates over weight and friction, and the snake flails without much net movement (part 2 in Supplementary Video 2). For relatively heavy snakes that are underpowered, friction dominates inertia, and the active torques simply uncoil the snake into a straight shape, again leading to little net movement (part 2 in Supplementary Video 2). However, for intermediate weights, the S-start leads to a finite propulsion speed. These possible biomechanical limits of S-starts show how juveniles can use S-starts for rapid escape, but lose that ability as they grow (Fig. 3c).

Having studied the regime in which S-starts are feasible from a biodynamical perspective, we now turn to consider the broader question of its relation to other non-planar snake gaits, of which the most famous is the eponymous sidewinding gait as it gives the illusion of a snake winding itself sideways[1]. In fact, during sidewinding, the snake lifts part of its body out of the plane, and places it askew periodically, and then propagates a localized bent and twisted region along its body, leading to net motion[8–12], raising questions about its origins, and limits from a dynamical, physiological and evolutionary perspective[13,35,36]. Just as in the S-start, sidewinding involves spatially inhomogeneous non-planar transient motions. So could the S-start serve as a building block of a sidewinding gait?

To probe this premise, we periodically initiate the spatiotemporal patterns of the torque triplets used for the S-start at the head and propagate them along the body (Supplementary Fig. 3a). We find that as this wave propagates along the snake, it causes the body to translate orthogonally to its tail-to-head direction, pivoting about multiple contact points that are themselves stationary with respect to the ground

https://doi.org/10.1038/s41567-025-02835-7

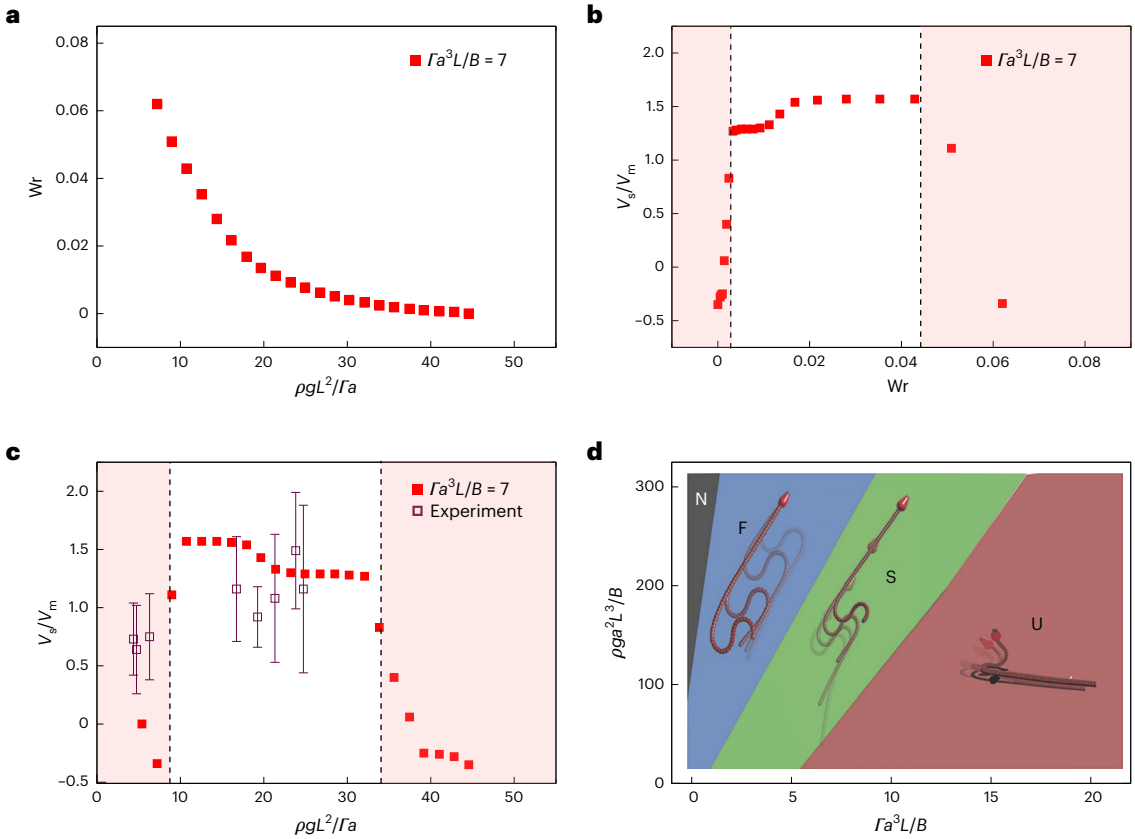

Fig. 3 | Topological dynamics and phase diagram for S-start. a, Snake centerline Wr that characterizes its non-planarity at one instant of time, as a function of its scaled body weight relative to muscular forces, $\rho gL^2/\Gamma a$, obtained from the simulations. As expected, Wr decreases monotonically with increasing weight and decreasing muscular forces. **b**, v_s/v_m as a function of body centerline Wr computed from the simulations. Below a certain Wr threshold, the snake fails to lift off the ground, and friction prohibits forward motion, and the snake straightens out as its centre of mass moves backwards. For an intermediate range of Wr values (unshaded region), the snake lifts off the ground without flailing, maximizing speed. Above a certain Wr threshold, the snake flails, assuming a disordered three-dimensional shape that fails to produce cohesive forward motion. **c**, Scaled forward snake speed as a function of the scaled body weight, obtained by combining the results shown in **a** and **b**. The filled symbols are simulation data and open symbols correspond to juvenile yellow anacondas (*E. notaeus*). The error bars corresponding to standard deviation obtained from averaging the scaled velocity of eight snakes measured on different surfaces (Supplementary Section I). The S-start fails for both small and large values of $\rho gL^2/\Gamma a$; heavy/weak snakes uncoil without any net forward translation, whereas light/strong snakes flail and move incoherently. Successful S-starts are possible for intermediate values of $\rho gL^2/\Gamma a$ that lead to intermediate values of Wr (marked as the unshaded region in **b**). **d**, A two-dimensional phase space indicates different locomotion regimes, characterized by two parameters, a scaled muscular torque $\Gamma a^3 L/B$ and scaled weight $\rho g a^2 L^3/B$, where B is the bending stiffness of the filament. Very small, strong snakes are inertially unstable (U), whereas large, heavy snakes are frictionally dominated (F) and move backwards, whereas extremely heavy and weak snakes, that is, $\rho g a^2 L^3/B \gg 1$ and $\Gamma a^3 L/B \approx 1$, cannot move at all (N). The S-start (S) is feasible only in the sweet spot of body weight and muscular forces (Supplementary Video 2).

(Supplementary Fig. 4 and Supplementary Video 3). Since sidewinding involves multiple λ pulses (Supplementary Figs. 2 and 4), each similar to an S-start profile propagating through the snake, the sidewinding gait might have evolved from the S-start. Bolstering this perspective, a recent study[14] reports an unusual arboreal mode of locomotion in climbing snakes facilitated by the propagation of strongly localized deformations. Videos of the gait indicate three-dimensional writhing and bending deformations, except now deployed by a snake wrapped around a cylindrical pole; these are qualitatively similar to periodic S-starts, but we defer a detailed study to the future. All together, the possible function of localized pulses such as the S-start as the basis for transient movements in many different snakes suggests the potential importance of λ pulses for the evolution and learning of a range of three-dimensional gaits in snakes.

More broadly, our study shows how developmental changes in animal size and shape lead to changes in the physical constraints that drive qualitative gait transitions. Understanding the biomechanical basis for the complex dynamics of contact of the snake with the substrate, the neuromechanical basis for the control of the S-start and the potential ability to translate our observations to engineering solutions of rapid non-planar modes in active slender systems seem like the natural next steps.

Online content

Any methods, additional references, Nature Portfolio reporting summaries, source data, extended data, supplementary information, acknowledgements, peer review information; details of author contributions and competing interests; and statements of data and code availability are available at https://doi.org/10.1038/s41567-025-02835-7.

References

1. Gray, J. *Animal Locomotion* (Norton,1968).
2. Marvi, H., Bridges, J. & Hu, D. Snakes mimic earthworms: propulsion using rectilinear travelling waves. *J. R. Soc. Interface* **10**, 20130188 (2013).
3. Gray, J. & Lissmann, H. The kinetics of locomotion of the grass-snake. *J. Exp. Biol.* **26**, 354–367 (1950).
4. Gasc, J., Cattaert, D., Chasserat, C. & Clarac, F. Propulsive action of a snake pushing against a single site: its combined analysis. *J. Morphol.* **201**, 315–329 (1989).

5. Moon, B. & Gans, C. Kinematics, muscular activity and propulsion in gopher snakes. *J. Exp. Biol.* **201**, 2669–2684 (1998).
6. Guo, Z. & Mahadevan, L. Limbless undulatory propulsion on land. *Proc. Natl Acad. Sci. USA* **105**, 3179–3184 (2008).
7. Hu, D., Nirody, J., Scott, T. & Shelley, M. The mechanics of slithering locomotion. *Proc. Natl Acad. Sci. USA* **106**, 10081–10085 (2009).
8. Alexander, R. *Principles of Animal Locomotion* (Princeton Univ. Press, 2013).
9. Biewener, A. & Patek, S. *Animal Locomotion* (Oxford Univ. Press, 2018).
10. Jayne, B. Kinematics of terrestrial snake locomotion. *Copeia* **1986**, 915–927 (1986).
11. Gans, C. & Kim, H. Kinematic description of the sidewinding locomotion of four vipers. *Isr. J. Zool.* **38**, 9–23 (1992).
12. Marvi, H. et al. Sidewinding with minimal slip: snake and robot ascent of sandy slopes. *Science* **346**, 224–229 (2014).
13. Jayne, B. What defines different modes of snake locomotion? *Integr. Comp. Biol.* **60**, 156–170 (2020).
14. Savidge, J., Seibert, T., Kastner, M. & Jayne, B. Lasso locomotion expands the climbing repertoire of snakes. *Curr. Biol.* **31**, R7–R8 (2021).
15. Yeaton, I., Ross, S., Baumgardner, G. & Socha, J. Undulation enables gliding in flying snakes. *Nat. Phys.* **16**, 974–982 (2020).
16. Fu, Q., Astley, H. & Li, C. Snakes combine vertical and lateral bending to traverse uneven terrain. *Bioinspir. Biomim.* **17**, 036009 (2022).
17. Gart, S., Mitchel, T. & Li, C. Snakes partition their body to traverse large steps stably. *J. Exp. Biol.* **222**, jeb185991 (2019).
18. Jayne, B. & Davis, J. Kinematics and performance capacity for the concertina locomotion of a snake (*Coluber constrictor*). *J. Exp. Biol.* **156**, 539–556 (1991).
19. Alfaro, M. Forward attack modes of aquatic feeding garter snakes. *Funct. Ecol.* **16**, 204–215 (2002).
20. Alfaro, M. Sweeping and striking: a kinematic study of the trunk during prey capture in three thamnophiine snakes. *J. Exp. Biol.* **206**, 2381–2392 (2003).
21. Vincent, S., Herrel, A. & Irschick, D. Comparisons of aquatic versus terrestrial predatory strikes in the pitviper, *Agkistrodon piscivorus*. *J. Exp. Zoo. A* **303A**, 476–488 (2005).
22. Alben, S. Efficient bending and lifting patterns in snake locomotion. *Proc. R. Soc. A* **478**, 20220312 (2022).
23. Domenici, P. & Blake, R. The kinematics and performance of fish fast-start swimming. *J. Exp. Biol.* **200**, 1165–1178 (1997).
24. Gazzola, M., Van Rees, W. & Koumoutsakos, P. C-start: optimal start of larval fish. *J. Fluid Mech.* **698**, 5–18 (2012).
25. Kolinski, J., Aussillous, P. & Mahadevan, L. Shape and motion of a ruck in a rug. *Phys. Rev. Lett.* **103**, 174302 (2009).
26. Rivas, J. et al. in *Biology Of The Boas And Pythons* (eds Henderson, R. W. & Powell, R.) 129–138 (Eagle Mountain Publishing, 2007).
27. Prange, H. & Christman, S. The allometrics of rattlesnake skeletons. *Copeia* **1976**, 542–545 (1976).
28. Anderson, J., Rahn, H. & Prange, H. Scaling of supportive tissue mass. *Q. Rev. Biol.* **54**, 139–148 (1979).
29. Garcia, G. & Silva, J. Interspecific allometry of bone dimensions: a review of the theoretical models. *Phys. Life Rev.* **3**, 188–209 (2006).
30. O'Reilly, O. M. *Modeling Nonlinear Problems in the Mechanics of Strings and Rods* (Springer, 2017).
31. Gazzola, M., Dudte, L., McCormick, A. & Mahadevan, L. Forward and inverse problems in the mechanics of soft filaments. *R. Soc. Open Sci.* **5**, 171628–171628 (2018).
32. Calugareanu, G. L'intégrale de Gauss et l'analyse des noeuds tridimensionnels. *Rev. Math. Pures Appl.* **4**, 5–20 (1959).
33. Ricca, R. & Nipoti, B. Gauss' linking number revisited. *J. Knot Theory Ramif.* **20**, 1325–1343 (2011).
34. Fuller, F. The writhing number of a space curve. *Proc. Natl Acad. Sci. USA* **68**, 815–819 (1971).
35. Tingle, J. Facultatively sidewinding snakes and the origins of locomotor specialization. *Int. Comp. Bio.* **60**, 202–214 (2020).
36. Jayne, B. Muscular mechanisms of snake locomotion: an electromyographic study of lateral undulation of the Florida banded water snake (*Nerodia fasciata*) and the yellow rat snake (*Elaphe obsoleta*). *J. Morphol.* **197**, 159–181 (1988).

Publisher's note Springer Nature remains neutral with regard to jurisdictional claims in published maps and institutional affiliations.

Springer Nature or its licensor (e.g. a society or other partner) holds exclusive rights to this article under a publishing agreement with the author(s) or other rightsholder(s); author self-archiving of the accepted manuscript version of this article is solely governed by the terms of such publishing agreement and applicable law.

© The Author(s), under exclusive licence to Springer Nature Limited 2025

Methods

Detailed description of the experimental methods, data analysis, mathematical model and simulation details are provided in the Supplementary Information.

Ethics statement

All experimental treatments were approved by the Institutional Animal Care and Use Committees (IACUCs) of Washburn University and the University of Massachusetts Lowell, as well as the Department of Wildlife and Fisheries, Commonwealth of Massachusetts. This study did not include any invasive methodology, and the study animals were not harmed in any way during the course of this study.

Reporting summary

Further information on research design is available in the Nature Portfolio Reporting Summary linked to this article.

Data availability

The data that support the findings of this study are available from the corresponding author upon request. Source data are provided with this paper.

Code availability

Code used for the simulation is available via GitHub at https://github.com/Chelakkot/S-start.

Acknowledgements

We thank NSF grants BioMatter DMR 1922321, MRSEC DMR 2011754 and EFRI 1830901, the Simons Foundation and the Henri Seydoux Fund (L.M.) for partial financial support.

Author contributions

B.Y. observed the escape behaviour and carried out the experiments with snakes. L.M. conceived and designed the study and approaches. N.C. performed the numerical simulations, in consultation with R.C., M.G. and L.M. L.M. conceived of the mathematical model, the phase space and the scaling laws. N.C., R.C. and L.M. wrote the paper. L.M. supervised the study.

Competing interests

The authors declare no competing interests.

Additional information

Supplementary information The online version contains supplementary material available at https://doi.org/10.1038/s41567-025-02835-7.

Correspondence and requests for materials should be addressed to L. Mahadevan.

Peer review information *Nature Physics* thanks the anonymous reviewers for their contribution to the peer review of this work.

Reprints and permissions information is available at www.nature.com/reprints.

nature portfolio

Corresponding author(s): L. Mahadevan

Last updated by author(s): Dec 6, 2024

Reporting Summary

Nature Portfolio wishes to improve the reproducibility of the work that we publish. This form provides structure for consistency and transparency in reporting. For further information on Nature Portfolio policies, see our Editorial Policies and the Editorial Policy Checklist.

Statistics

For all statistical analyses, confirm that the following items are present in the figure legend, table legend, main text, or Methods section.

n/a	Confirmed
☐	☒ The exact sample size (*n*) for each experimental group/condition, given as a discrete number and unit of measurement
☐	☒ A statement on whether measurements were taken from distinct samples or whether the same sample was measured repeatedly
☒	☐ The statistical test(s) used AND whether they are one- or two-sided *Only common tests should be described solely by name; describe more complex techniques in the Methods section.*
☒	☐ A description of all covariates tested
☒	☐ A description of any assumptions or corrections, such as tests of normality and adjustment for multiple comparisons
☒	☐ A full description of the statistical parameters including central tendency (e.g. means) or other basic estimates (e.g. regression coefficient) AND variation (e.g. standard deviation) or associated estimates of uncertainty (e.g. confidence intervals)
☒	☐ For null hypothesis testing, the test statistic (e.g. *F*, *t*, *r*) with confidence intervals, effect sizes, degrees of freedom and *P* value noted *Give P values as exact values whenever suitable.*
☒	☐ For Bayesian analysis, information on the choice of priors and Markov chain Monte Carlo settings
☒	☐ For hierarchical and complex designs, identification of the appropriate level for tests and full reporting of outcomes
☒	☐ Estimates of effect sizes (e.g. Cohen's *d*, Pearson's *r*), indicating how they were calculated

Our web collection on statistics for biologists contains articles on many of the points above.

Software and code

Policy information about availability of computer code

Data collection	All codes are made available in the repository https://github.com/Chelakkot/S-start
Data analysis	All data analysis protocols are described in the paper Source files for Figure 1:https://zenodo.org/records/14535342? token=eyJhbGciOiJIUzUxMiJ9.eyJpZCI6IjY5MzM4NGZjLTZkYzctNDk1OS04ZmU4LTA2ZDM2ODgwNDcwYyIsImRhdGEiOnt9LCJyYW5kb20iOiI0ZDI1MGE5MzllMmUyYTI1OTRhNTZkYTE0Nzg2ZGY5NyJ9.DqD6O7ZCjPy-- Wx8pnO9TB9EnVLKWScldb9oYH_FNPV6FX9rIcIPiTZNe_P7qsKn5GAhZJlmK7CrvNThFSmhhA Source data for figure 2: https://zenodo.org/records/14535372? token=eyJhbGciOiJIUzUxMiJ9.eyJpZCI6ImM4NjQxMDA3LTQyOTMtNDM0NC04YTQ3LTNiZTBjYjkwYmNkMiIsImRhdGEiOnt9LCJyYW5kb20iOiI0ZTYxOTdkMWI4ZGFjOTBkNDQ5MDJlNTQyZGMwNmU2MyJ9.61yV0KD2fid2cAQIB2VrEgCeEIRQzsfDFYsXOWCTPnIf31SXxggrTWUuvmVwZ_H5Zl6mDkXDiAl5c0ae0Wk5mA Source data for Figure 3: https://zenodo.org/records/14535385? token=eyJhbGciOiJIUzUxMiJ9.eyJpZCI6IjBkNDdkNWQ1LTNhNzktNGRlOS04ZDgyLTE4ZTE0OWE2MDEwMyIsImRhdGEiOnt9LCJyYW5kb20iOiIxMmUxZTRhMjJlZjRmYzYxNDU1MjI2MTU3MDY1NWQxNiJ9.YzNSV-2A0tIHXn0XAu3nuObbWC0mXKlZIjXUkskWDL2efdirAAsq_hGTgNyt8gfn_79c1m1DNhezN1Fl-toR6Q

For manuscripts utilizing custom algorithms or software that are central to the research but not yet described in published literature, software must be made available to editors and reviewers. We strongly encourage code deposition in a community repository (e.g. GitHub). See the Nature Portfolio guidelines for submitting code & software for further information.

Data

Policy information about availability of data

All manuscripts must include a data availability statement. This statement should provide the following information, where applicable:

- Accession codes, unique identifiers, or web links for publicly available datasets
- A description of any restrictions on data availability
- For clinical datasets or third party data, please ensure that the statement adheres to our policy

All data and codes will be made available via public repositories upon publication.

Research involving human participants, their data, or biological material

Policy information about studies with human participants or human data. See also policy information about sex, gender (identity/presentation), and sexual orientation and race, ethnicity and racism.

Reporting on sex and gender	na
Reporting on race, ethnicity, or other socially relevant groupings	na
Population characteristics	na
Recruitment	na
Ethics oversight	na

Note that full information on the approval of the study protocol must also be provided in the manuscript.

Field-specific reporting

Please select the one below that is the best fit for your research. If you are not sure, read the appropriate sections before making your selection.

☒ Life sciences ☐ Behavioural & social sciences ☐ Ecological, evolutionary & environmental sciences

For a reference copy of the document with all sections, see nature.com/documents/nr-reporting-summary-flat.pdf

Life sciences study design

All studies must disclose on these points even when the disclosure is negative.

Sample size	Locomotor trials were performed on ten newborn, five juvenile, and two adult specimens of the yellow anaconda. The locomotor mode we describe in the manuscript was observed in all ten newborns and all five juveniles; that sample size was considered adequate for us to claim that this mode of locomotion is present in this species of snake.
Data exclusions	No data were excluded from the analysis
Replication	All locomotor trials were replicated with the juvenile and newborn snakes. Our attempts to replicate the locomotion with the larger snakes failed. That finding is reported in the manuscript and its significance detailed.
Randomization	Randomization was not relevant for this study; all of the specimens were given multiple opportunities to locomote. There was no "order bias" to their modes of locomotion.
Blinding	There were no group allocations for data analysis, so blinding was not necessary.

Reporting for specific materials, systems and methods

We require information from authors about some types of materials, experimental systems and methods used in many studies. Here, indicate whether each material, system or method listed is relevant to your study. If you are not sure if a list item applies to your research, read the appropriate section before selecting a response.

Materials & experimental systems

n/a	Involved in the study
☒	☐ Antibodies
☒	☐ Eukaryotic cell lines
☒	☐ Palaeontology and archaeology
☐	☒ Animals and other organisms
☒	☐ Clinical data
☒	☐ Dual use research of concern
☒	☐ Plants

Methods

n/a	Involved in the study
☒	☐ ChIP-seq
☒	☐ Flow cytometry
☒	☐ MRI-based neuroimaging

Animals and other research organisms

Policy information about studies involving animals; ARRIVE guidelines recommended for reporting animal research, and Sex and Gender in Research

Laboratory animals	Study did not involve laboratory animals.
Wild animals	Study did not involve wild animals. The yellow anacondas (Eunectes notaeus) used for the study were captive-bred in the United States and obtained commercially.
Reporting on sex	The sex of the animals were undetermined
Field-collected samples	No field-collected samples were incorporated into this study
Ethics oversight	This study was approved by the IACUC of Washburn University as well as the IACUC of University of Massachusetts Lowell.

Note that full information on the approval of the study protocol must also be provided in the manuscript.

Plants

Seed stocks	na
Novel plant genotypes	na
Authentication	na